

Article

# Heteroaggregation and Homoaggregation of Latex Particles in the Presence of Alkyl Sulfate Surfactants

Tianchi Cao <sup>1,2</sup>, Michal Borkovec <sup>1</sup> and Gregor Trefalt <sup>1,\*</sup> 

<sup>1</sup> Department of Inorganic and Analytical Chemistry, University of Geneva, Sciences II, 30 Quai Ernest-Ansermet, 1205 Geneva, Switzerland; tianchi.cao@yale.edu (T.C.); michal.borkovec@unige.ch (M.B.)

<sup>2</sup> Department of Chemical and Environmental Engineering, Yale University, New Haven, CT 06520, USA

\* Correspondence: gregor.trefalt@unige.ch

Received: 19 October 2020; Accepted: 6 November 2020; Published: 13 November 2020



**Abstract:** Heteroaggregation and homoaggregation is investigated with time-resolved multi-angle dynamic light scattering. The aggregation rates are measured in aqueous suspensions of amidine latex (AL) and sulfate latex (SL) particles in the presence of sodium octyl sulfate (SOS) and sodium dodecyl sulfate (SDS). As revealed by electrophoresis, the surfactants adsorb to both types of particles. For the AL particles, the adsorption of surfactants induces a charge reversal and triggers fast aggregation close to the isoelectric point (IEP). The negatively charged SL particles remain negatively charged and stable in the whole concentration range investigated. The heteroaggregation rates for AL and SL particles are fast at low surfactant concentrations, where the particles are oppositely charged. At higher concentrations, the heteroaggregation slows down above the IEP of the AL particles, where the particles become like-charged. The SDS has higher affinity to the surface compared to the SOS, which induces a shift of the IEP and of the fast aggregation regime to lower surfactant concentrations.

**Keywords:** colloidal stability; heteroaggregation; DLVO

## 1. Introduction

Aggregation of particles in suspensions is important in many practical applications, such as ceramic processing, paint fabrication, or drug formulation [1–4]. Many of these applications involve a mixture of different types of particles. This fact implies that one needs to understand not only homoaggregation (i.e., aggregation between similar particles), but also heteroaggregation (i.e., aggregation between dissimilar particles). While homoaggregation is a relatively well studied topic, heteroaggregation is much less investigated. Some quantitative studies of heteroaggregation involving oppositely charged particles have been published recently [5,6]. The situation, where one of the particles undergoes a charge reversal results in a very rich behavior, where homoaggregation and heteroaggregation run in parallel. Only few studies analyze such systems quantitatively [7–10].

One of the possibilities to control particle aggregation is by means of surfactants [11–19]. Normally, surfactants with an opposite sign of charge to the charge of the particles are used. In such systems, the surfactant in question adsorbs to the particle surface and induces a charge reversal [13,15,17,19]. In such systems, homoaggregation was studied for positively charged particles in the presence of alkyl sulfates or fatty acids, while for negative particles in the presence of alkyl amines [12–16]. All these studies report a similar aggregation behavior. At low surfactant concentrations, particles are highly charged and the particle suspension is stable. By increasing the surfactant concentration, the particles become neutral at the isoelectric point (IEP). In the vicinity of this point, the particles aggregate rapidly. Even higher surfactant concentrations induce a charge reversal and a re-stabilization of the suspension. The region of fast aggregation is typically quite narrow, and is centered around the IEP. For this reason, precise surfactant dosing is necessary in order to induce fast aggregation. It was further shown that

with increasing length of the surfactant alkyl chain the IEP and the unstable region shift to lower concentrations [12,13,15]. A similar behavior was observed for ionic liquid constituents, some of which can be regarded as short-chain surfactants [20].

These findings only concern homoaggregation, while data on heteroaggregation in such surfactant systems hardly exist. To our knowledge, the only exception is our recent study of latex particles in the presence of sodium octyl sulfate [8]. The goal of that study was to develop a novel methodology, which enables measurements of slow heteroaggregation rates in the presence of fast homoaggregation, as this situation becomes relevant in these systems. This technique is based on multi-angle time-resolved light scattering, and allows extracting heteroaggregation rates with good precision even in samples, where homoaggregation dominates. This selectivity is achieved by optimizing the mutual contrast of the particles involved, which is achieved by choosing an appropriate size and concentration ratio.

The goal of the present contribution is to apply the method developed in Ref. [8] to study both homoaggregation and heteroaggregation in the presence of different alkyl sulfate surfactants. In particular, we compare the effect of two alkyl sulfates of different chain length on the heteroaggregation process in the mixture of amidine latex (AL) and sulfate latex (SL) particles. We further complement these experiments with studies of the respective homoaggregation process and electrophoresis. The experimental findings are finally compared with calculations based on the theory by Derjaguin, Landau, Verwey, and Overbeek (DLVO) [21,22].

The particles used in the present study are the same as the ones used originally in our earlier study of particle homoaggregation in the presence of tetraphenylborate anions [23]. This publication also provides more details on the particle characterization.

## 2. Materials and Methods

### 2.1. Materials

Suspensions of amidine latex (AL) and sulfate latex (SL) particles were purchased from Thermo Fischer (product numbers: AL: A37315, SL: S37491). The radii of the AL and SL particles are 149 nm and 117 nm, respectively. These radii were determined by static light scattering and reported in our earlier work [23]. The particle suspensions were dialyzed in polyvinylidene fluoride (for AL particles) and cellulose ester (for SL particles) membranes against Milli-Q water (Millipore), until the electrical conductivity was below about 80  $\mu\text{S}/\text{m}$ . This value of conductivity suggests that charged impurities were successfully removed. The pH of all suspensions was adjusted to pH 4.0 by adding appropriate amount of HCl. Analytical grade sodium octyl sulfate (SOS, Alfa Aesar) and sodium dodecyl sulfate (SDS, Sigma-Aldrich) were used as additives for controlling aggregation processes. The background electrolyte concentration was adjusted by adding NaCl (Sigma Aldrich) to the suspensions. All solutions were prepared with Milli-Q. Experiments were carried out at a temperature of 25 °C.

### 2.2. Electrophoresis

A ZetaSizer NanoZS (Malvern Instruments) was used to measure the electrophoretic mobility of the AL and SL particles in suspensions with different solution conditions. In solutions of simple electrolytes (e.g., NaCl) the AL particles are positively charged, while the SL particles negatively. The suspensions were prepared by mixing the particle stock suspension with the solution containing the desired amount of SOS or SDS, and NaCl. The particle concentrations in the suspensions were 0.50 mg/L ( $3.4 \cdot 10^{-14} \text{m}^{-3}$ ) and 0.23 mg/L ( $3.3 \cdot 10^{-14} \text{m}^{-3}$ ) for the AL and SL particles, respectively. The electrokinetic potential ( $\zeta$ -potential) was obtained from the measured electrophoretic mobility with the model developed by O'Brien and White [24].

### 2.3. Measuring and Extracting Aggregation Rates

Particle aggregation was studied using a multiangle goniometer (ALV/CGS-8F) equipped with eight fiber optic detectors and a solid-state laser with a wavelength of 532 nm. The angular resolution of  $4.25^\circ$  was used. The experiments were conducted in borosilicate cuvettes (Kimberly Chase). The cuvettes were first treated in hot piranha solution, which is a mixture of 30%  $\text{H}_2\text{O}_2$  and 96%  $\text{H}_2\text{SO}_4$  in a volume ratio of 1:3. Then, they were thoroughly washed with Milli-Q water and dried in a dust-free oven. The sample preparation and the particle concentration are the same as those in the above electrophoresis experiments. For homoaggregation measurements, the light scattering signals were recorded at scattering angle of  $90^\circ$  and accumulated for 20 s. The information of hydrodynamic radius was obtained by analyzing the correlation functions with a second-order cumulant fit. The hydrodynamic radii were measured within their increase less than 30% since only the early stages of the aggregation process are investigated. For heteroaggregation experiments, the mixture of AL (0.50 mg/L) and SL (0.23 mg/L) particles were monitored at different scattering angles. The apparent dynamic rate was extracted by fitting the initial dependence of the hydrodynamic radius on time with a straight line.

The aggregation rates are measured in two types of samples. In the first case only one type of particles, A, are present and from these experiments homoaggregation rates are determined. Note that in the present data set homoaggregation is observed only for amidine latex particles, while sulfate latex particles are stable against homoaggregation in the whole range of salt concentrations. For measuring homoaggregation rates we employ single angle time-resolved dynamic light scattering. The apparent dynamic rate,  $\Delta$ , which corresponds to the relative rate of increase of hydrodynamic radius,  $R_h$ , is first extracted

$$\Delta(t, Q) = \frac{1}{R_h(0, Q)} \cdot \left. \frac{dR_h(t, Q)}{dt} \right|_{t=0} \quad (1)$$

where  $t$  is the time,  $Q = 4\pi/\lambda \sin(\theta/2)$  is the magnitude of the scattering vector with  $\lambda$  and  $\theta$  being wavelength of the light in medium and scattering angle, respectively. The homoaggregation stability ratio is then calculated using equation

$$W_{ij} = \frac{\Delta_{ij}^{(\text{fast})}}{\Delta_{ij}}, \quad (2)$$

where subscript  $ij$  denotes the particle pair. For homoaggregation of particles of type A, one has  $i = j = A$ . The superscript (fast) refers to the diffusion controlled rate measured in 0.8 M NaCl. The absolute aggregation rates are calculated as

$$k_{ij} = \frac{k_{ij}^{(\text{fast})}}{W_{ij}}, \quad (3)$$

where  $k_{ij}^{(\text{fast})}$  is the fast absolute rate. The fast rates for homoaggregation of amidine and sulfate particles used in this work are  $(3.1 \pm 0.2) \cdot 10^{-18} \text{ m}^3/\text{s}$  and  $(2.8 \pm 0.2) \cdot 10^{-18} \text{ m}^3/\text{s}$ , respectively. These values were measured by multi-angle dynamic light scattering and extracted with T-matrix calculations as reported elsewhere [8].

For heteroaggregation rate measurements, AL and SL suspensions are mixed, which results in suspension containing two types of particles, namely A and B. Here three types of aggregates, AA, BB, and AB can form between two types of particles A and B. When the apparent dynamic rate of such a mixture is measured all three types of aggregates contribute to the total rate

$$\Delta(Q) = k_{AA}H_{AA}(Q) + 2k_{AB}H_{AB}(Q) + k_{BB}H_{BB}(Q), \quad (4)$$

where  $k_{ij}$  are the absolute aggregation rates for particle pair  $ij$  and the  $H_{ij}$  are functions, which depend on optical properties of the respective particles and their concentrations. These functions are calculated with T-matrix theory and low Reynolds hydrodynamics for spherical particles as described in

Refs. [7,25]. The apparent dynamic rates for mixtures of AL and SL particles are measured as a function of scattering vector and fitted to Equation (4). The homoaggregation rates  $k_{AA}$  are measured in separate homoaggregation experiments for the same conditions, while  $k_{BB}$  is set to zero, since SL particles are stable in all conditions. This leaves us with only one unknown parameter  $k_{AB}$  in Equation (4), therefore the absolute rate for heteroaggregation can reliably be determined [8]. Examples of apparent dynamic rates for the mixture of AL and SL particles as a function of the magnitude of the scattering vector  $Q$  for different concentrations of sodium octyl sulfate are shown in Figure 1.

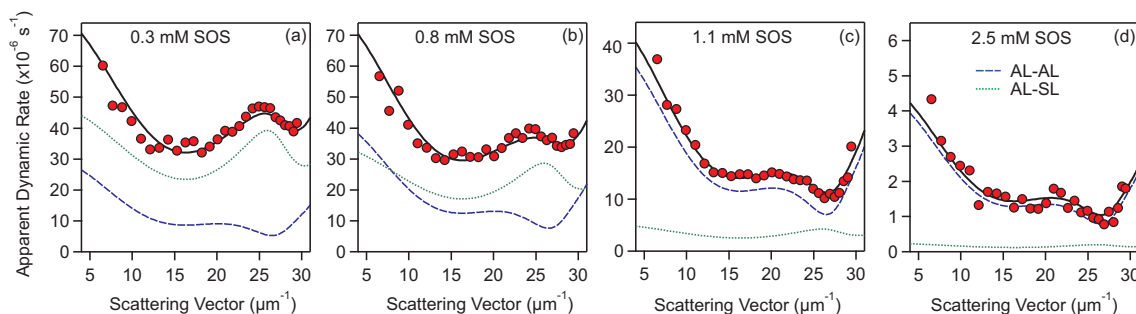


**Figure 1.** Apparent dynamic rates for the mixture of AL and SL particles as a function of the magnitude of the scattering vector  $Q$  at (a) 0.3 mM, (b) 0.8 mM, (c) 1.1 mM, and (d) 2.5 mM SOS. The symbols are experimentally determined apparent rates, while full line represents the fit to Equation (4). The dotted and dashed lines represent the contribution of AL-AL and AL-SL aggregates, respectively. The particle concentrations used are 0.50 mg/L ( $3.4 \cdot 10^{-14} \text{m}^{-3}$ ) and 0.23 mg/L ( $3.3 \cdot 10^{-14} \text{m}^{-3}$ ) for AL and SL, respectively.

The experimental points shown with symbols can be accurately fitted with Equation (4). Only contributions of AL-AL and AL-SL aggregates are present, since the SL particles do not undergo homoaggregation. The AL and SL particle sizes as well as their number fractions are chosen such that the optimal sensitivity for AL-SL heteroaggregation is achieved. A signature of strong contribution of AL-SL heteroaggregation is the peak observed at  $Q \approx 25 \mu\text{m}^{-1}$ , while at this  $Q$  the apparent rate from AL-AL homoaggregation has a minimum. This feature enables to extract heteroaggregation rates accurately even in the presence of fast homoaggregation process. At 0.3 mM of SOS the aggregation process is dominated by the formation of AL-SL aggregates as evident from the pronounced peak at  $Q \approx 25 \mu\text{m}^{-1}$ . With increasing the SOS concentration, the contribution of AL-SL aggregates is decreased and at 2.5 mM SOS, the aggregation is almost fully dominated by AL-AL homoaggregation, see Figure 1d. Albeit in the later case the heteroaggregation rate coefficient is very small, it can still be reliably extracted from the experimentally determined apparent dynamic rates.

The apparent dynamic rates for aggregation of mixture of AL and SL particles in the presence of SDS are shown in Figure 2. A very similar behavior compared to the SOS case is observed, except that the transition from heteroaggregation to homoaggregation dominated regime is shifted to much lower surfactant concentrations. At 1.0  $\mu\text{M}$  of SDS the signal is mainly due to the formation of AL-SL heteroaggregates. Again, with increasing concentration the contribution of AL-SL aggregates is decreased and at 6.7  $\mu\text{M}$  of SDS, the signal is almost completely due to AL-AL homoaggregation process.

The analysis explained above and shown in Figures 1 and 2 permits us to extract the heteroaggregation rate coefficient,  $k_{AB}$ , at every concentration of the surfactant. Finally these absolute heteroaggregation rate coefficients are converted into stability ratios for heteroaggregation via Equation (2). The fast heteroaggregation rate coefficient  $k_{AB}^{(\text{fast})}$  was determined in 0.8 M NaCl and is equal to  $(3.1 \pm 0.2) \cdot 10^{-18} \text{m}^3/\text{s}$  [8].

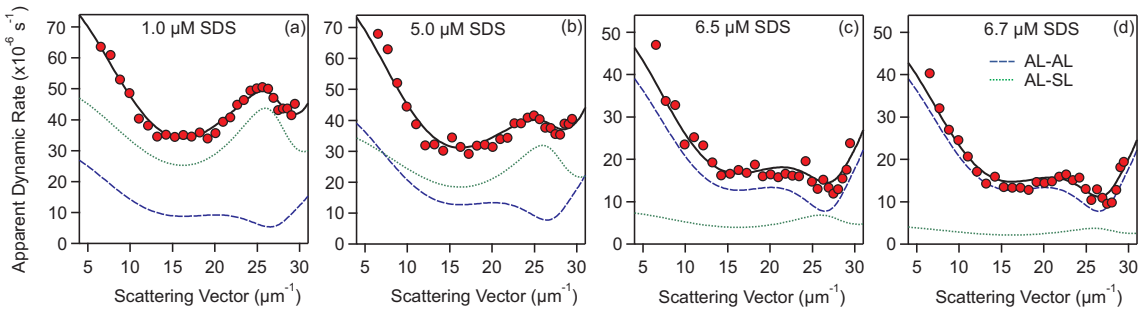


**Figure 2.** Apparent dynamic rates for the mixture of AL and SL particles as a function of the magnitude of the scattering vector  $Q$  at (a) 1.8  $\mu\text{M}$ , (b) 5.0  $\mu\text{M}$ , (c) 6.5  $\mu\text{M}$ , and (d) 6.7  $\mu\text{M}$  SDS. The symbols are experimentally determined apparent rates, while full line represents the fit to Equation (4). The dotted and dashed lines represent the contribution of AL-AL and AL-SL aggregates. The particle concentrations used are 0.50 mg/L ( $3.4 \cdot 10^{-14} \text{m}^{-3}$ ) and 0.23 mg/L ( $3.3 \cdot 10^{-14} \text{m}^{-3}$ ) for AL and SL, respectively.

#### 2.4. Calculating Aggregation Rates with DLVO Theory

Consider the pressure  $\Pi$  between two planar surfaces, which is assumed to be dominated by van der Waals and double-layer interactions [26,27]

$$\Pi = \Pi_{\text{vdW}} + \Pi_{\text{dl}}, \quad (5)$$

where  $\Pi_{\text{vdW}}$  and  $\Pi_{\text{dl}}$  are the van der Waals and double-layer components of the pressure, respectively. The van der Waals pressure is approximated as [27]

$$\Pi_{\text{vdW}} = -\frac{H}{6\pi} \cdot \frac{1}{h^3}, \quad (6)$$

where  $h$  is the distance between the plates and  $H$  the Hamaker constant. In all the calculations, the Hamaker constant is set to  $3.1 \cdot 10^{-21} \text{J}$  [23]. Double-layer pressure is calculated by numerically solving the Poisson-Boltzmann (PB) equation

$$\frac{d^2\psi}{dx^2} = \frac{\kappa^2}{\beta q} \sinh(\beta q \psi), \quad (7)$$

where  $\psi(x)$  is the electrostatic potential profile between the plates located at  $x = \pm h/2$ ,  $\beta = 1/(k_B T)$  is the inverse thermal energy with  $T$  being the temperature and  $k_B$  the Boltzmann constant,  $q$  is the elementary charge, and  $\kappa$  is the inverse Debye length. The latter parameter is calculated via

$$\kappa^2 = \frac{2\beta q^2 c}{\epsilon_0 \epsilon_r}, \quad (8)$$

where  $c$  is the number concentration of monovalent electrolyte,  $\epsilon_0$  is the vacuum permittivity and  $\epsilon_r = 80$  is the relative permittivity of water at 25 °C. The PB equation is solved with the following boundary conditions [28]

$$\pm \epsilon_0 \epsilon_r \left. \frac{d\psi}{dx} \right|_{x=\pm h} = \sigma_{\pm} - C_{\text{in}}^{(\pm)} [\psi(\pm h/2) - \psi_{\pm}], \quad (9)$$

where  $\sigma_{\pm}$ ,  $\psi_{\pm}$ , and  $C_{\text{in}}^{(\pm)}$  are surface charge density, diffuse layer potential, and inner layer capacitance of the isolated plates. The surface charge density and diffuse layer potential are connected through charge-potential relationship [27]

$$\sigma_{\pm} = \frac{2\epsilon_0 \epsilon_r \kappa}{\beta q} \sinh\left(\frac{\beta q \psi_{\pm}}{2}\right). \quad (10)$$

Instead of the inner layer capacitance the regulation parameter is used [28]

$$p_{\pm} = \frac{C_{dl}^{(\pm)}}{C_{dl}^{(\pm)} + C_{in}^{(\pm)}}, \quad (11)$$

where  $C_{dl}^{(\pm)}$  is the diffuse layer capacitance of the isolated plate and can be calculated as [28]

$$C_{dl}^{(\pm)} = \varepsilon_0 \varepsilon_r \kappa \cosh\left(\frac{\beta q \psi_{\pm}}{2}\right). \quad (12)$$

This parameter assumes simple values for the classical boundary conditions of constant charge (CC,  $p = 1$ ) and constant potential (CP,  $p = 0$ ). We model intermediate regulation behavior by choosing  $p = 0.5$ . Note that within this model both the surface charge density and the potential of the plates vary with the separation distance. The solution of PB equation yields the potential profile between the plates  $\psi(x)$ , which is used to calculate the diffuse layer pressure [27]

$$\Pi_{dl} = 2k_B T c [\cosh(\beta q \psi) - 1] - \frac{\varepsilon_0 \varepsilon_r}{2} \left(\frac{d\psi}{dx}\right)^2. \quad (13)$$

The interaction energy between two spherical particles can be obtained by double integration of the pressure by means of the Derjaguin approximation [26,27]

$$V_{ij} = 2\pi R_{eff}^{(ij)} \int_h^{\infty} \int_{h'}^{\infty} \Pi(h'') dh'' dh', \quad (14)$$

where  $R_{eff}^{(ij)} = R_i R_j / (R_i + R_j)$  is the effective radius, with  $R_i$  and  $R_j$  being the radii of the respective particles. Note that in this case  $h$  is the smallest surface-to-surface separation distance between the spheres. Experimental values for radii of the AL and SL particles determined by SLS are used. The diffuse layer potentials are approximated with the experimentally measured electrokinetic potentials interpolated with empirical functions shown in Figures 3 and 4.

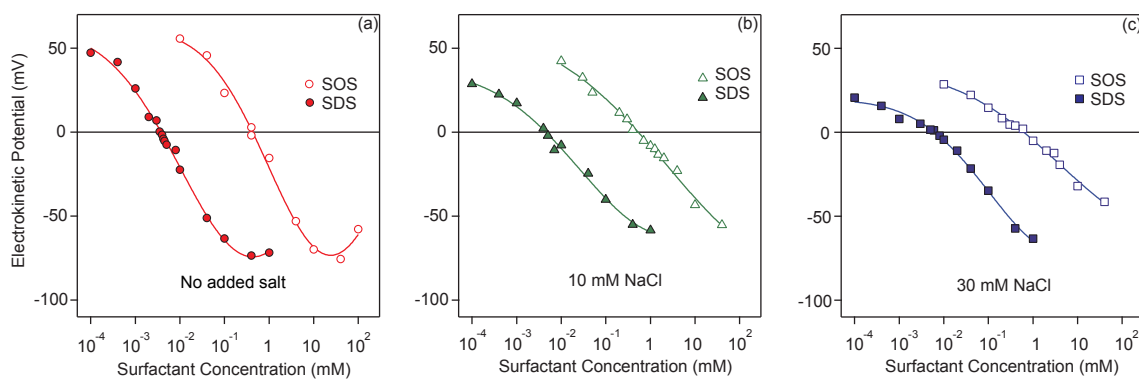


**Figure 3.** Electrokinetic potential of amidine latex particles as a function of surfactant concentration with (a) no added salt, (b) 10 mM NaCl, and (c) 30 mM NaCl. Empty symbols represent SOS and full symbols SDS surfactants. The lines are empirical interpolation functions.

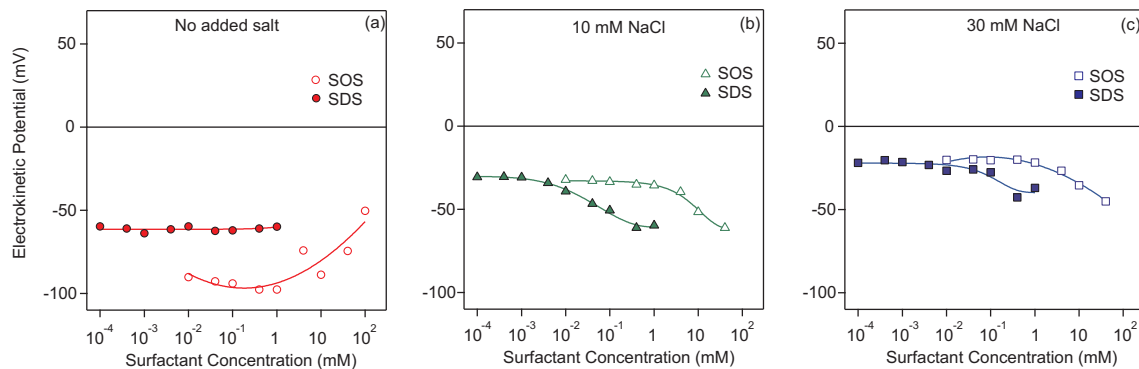


**Figure 4.** Electrokinetic potential of sulfate latex particles as a function of surfactant concentration with (a) no added salt, (b) 10 mM NaCl, and (c) 30 mM NaCl. Empty symbols represent SOS and full symbols SDS surfactants. The lines are empirical interpolation functions.

The aggregation rate coefficient is obtained by solving the steady-state diffusion equation, which yields [27]

$$k_{ij} = \frac{2k_B T}{3\eta R_{\text{eff}}^{(ij)}} \left[ \int_0^\infty \frac{B_{ij}(h) e^{\beta V_{ij}(h)} dh}{(R_i + R_j + h)^2} \right]^{-1}, \quad (15)$$

where hydrodynamic resistance function  $B_{ij}$  is approximated as [29]

$$B_{ij}(h) = \frac{6h^2 + 26R_{\text{eff}}^{(ij)}h + 8(R_{\text{eff}}^{(ij)})^2}{6h^2 + 8R_{\text{eff}}^{(ij)}h} \quad (16)$$

Finally the stability ratio is calculated via Equation (2). The fast rate coefficient  $k_{ij}^{(\text{fast})}$  is obtained by taking only the van der Waals attraction into account.

### 3. Results and Discussion

We report experimentally measured homoaggregation and heteroaggregation stability ratios in aqueous suspensions of amidine latex (AL) and sulfate latex (SL) particles in the presence of two different alkyl sulfate surfactants, namely sodium octyl sulfate (SOS) and sodium dodecyl sulfate (SDS). We first investigate the charging of both type of particles at different background salt concentrations by electrophoresis. Subsequently, we address the dependence of the stability ratios for homoaggregation and heteroaggregation on the surfactant concentration. These results are further confronted with theoretical predictions based on the DLVO theory. Finally, comparison with literature data is being made. Note that the data involving SOS were published in Ref. [8], but they are shown here again for the ease of comparison.

#### 3.1. Charging of the Particles in the Presence of Surfactants

The electrophoretic mobility of the AL and SL particles was measured with electrophoretic light scattering, and the mobilities were subsequently converted to electrokinetic potentials ( $\zeta$ -potential). Let us first consider the charging of AL particles in the presence of both surfactants, see Figure 3.

At very low surfactant concentration, AL particles are positively charged as expected from their surface chemistry and their charging behavior in NaCl solutions. Increasing of the surfactant concentration, the AL particles get progressively neutralized. The isoelectric point (IEP) point is reached at 0.5 mM and 5  $\mu\text{M}$  in the presence of SOS and SDS, respectively. Above these concentrations, the AL particles become negatively charged and their electrokinetic potential is decreasing with increasing concentration. When the concentration of background NaCl solution is increased, the qualitative behavior remains the same, albeit the magnitude of the electrokinetic potential is reduced due to additional screening. The charging of the AL particles is similar in both surfactant solutions,

except for its shift of about two orders of magnitude to lower concentrations for the SDS as compared to SOS. This shift indicates that the affinity of SDS towards the AL particles is substantially larger than for SOS. For both surfactants, the position of the IEP increases only very modestly with the background salt level, which indicates that the surfactant adsorption is mainly driven by non-electrostatic interactions. In all cases shown in Figure 3 the electrokinetic potential is constant or slightly decreasing. There is one exception, however, in the case of SOS surfactant with no added salt, the potential is increasing with increasing SOS concentration. Similar behavior was observed with the same particles in the presence of hydrophobic tetraphenylborate ions earlier [23]. This increase is probably a result of interplay of strong adsorption of hydrophobic ion on the surface and simultaneous screening of the double layer with increasing ion concentration.

The electrokinetic potentials for SL particles in the presence of surfactants are shown in Figure 4. The SL particles remain negatively charged in the whole range of surfactant and background salt concentrations studied. Again, the qualitative picture is similar for both surfactants, whereby the curves are shifted to lower concentrations for the SDS as compared to SOS. For the samples with no added salt the electrokinetic potential is increasing with increasing SOS concentration, while it stays constant at about  $-60$  mV in the presence of SDS. With increasing salt background concentration, the potential decreases with increasing surfactant concentration for both SOS and SDS. The decrease of the potential with surfactant concentration indicates that the negatively charged surfactants adsorb to negatively charged SL particles too. This behavior further confirms the previous observation that the surfactant adsorption on latex particles is mainly driven by non-electrostatic interactions.

### 3.2. Homoaggregation

Let us now address homoaggregation of the latex particles in the presence of alkyl sulfate surfactants. As shown in Figure 4 the SL particles are negatively charged at all investigated conditions. Light scattering experiments have confirmed that SL particles are stable and do not aggregate for all conditions investigated. On the other hand, the AL particles undergo a charge reversal upon addition of surfactants. Therefore, one expects fast homoaggregation near the IEP for the AL system. This feature is indeed evident in Figure 5, which shows the stability ratios for homoaggregation of AL particles in the presence of SOS and SDS.

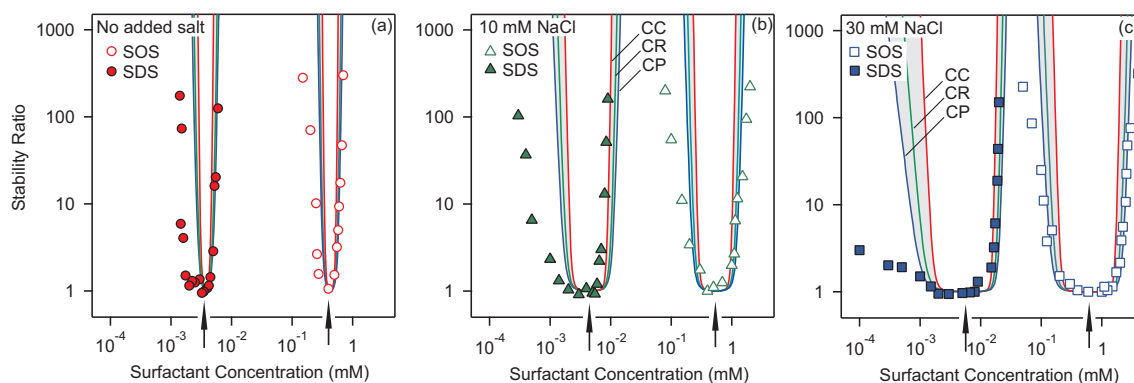


**Figure 5.** Stability ratios for homoaggregation of AL particles in the presence of SOS and SDS with (a) no added NaCl, (b) 10 mM NaCl, and (c) 30 mM NaCl added. Symbols represent experimental data, while lines show calculations based on DLVO theory. CC, CR, and CP labels mark constant charge, constant regulation, and constant potential boundary conditions. For the CR model the regulation parameters for both particles are equal to 0.5. The IEPs are indicated with arrows.

One observes the typical U-shaped curves for the stability ratio for both type of surfactants and different background electrolyte concentrations. The suspensions are stable at low surfactant concentrations, due to strong electrostatic repulsion that is induced by the high positive charge of the AL particles. The stability ratios decrease with increasing concentration before reaching a minimum close to the IEP. Near this point the stability ratios are close to unity, and the aggregation is close to

diffusion controlled. When the surfactant concentration is increased further, the particles progressively accumulate negative charge. This accumulation of charge again induces repulsive double layer forces, which result in the re-stabilization of the suspension, and an increase of the stability ratio. The behavior is qualitatively similar for both SOS and SDS surfactants. However, the curves corresponding to SDS are shifted to lower concentrations with respect to those of the SOS. This shift reflects the corresponding shift in the IEP as discussed above. Another feature that can be observed by comparing the panels (a) to (c) in Figure 5 is that with increasing background electrolyte concentration the unstable regions become wider. This effect is caused by the increased screening of the double layer forces with increasing electrolyte concentration.

Comparison of experimental and calculated stability ratios reveals that the DLVO theory explains the stability of AL particles reasonably well. The theory reproduces all qualitative features, especially the U-shaped stability curves, their position, and the increase of their width with increasing salt concentration. However, the quantitative agreement is not always perfect. The largest discrepancies between theory and experiment are observed for SDS at concentrations below the charge reversal, where the theory overestimates the stability ratio. These discrepancies could be caused by charge heterogeneities [30]. The discrepancy between theory and experiment is further reflected in the symmetry of the stability curves around the IEP. While theoretical stability curves are almost symmetric around the IEP, this is not the case for experimental curves, especially for the SDS surfactant. In the SDS system, the measured stability ratios are much smaller below the IEP than above. Below the IEP, the AL particles are positively charged, while negatively above the IEP. Similar asymmetries in the stability curves were observed for hematite particles by changing the pH [31], latex particles with adsorbed dendrimers [32], or in the presence of alkyl sulfate surfactants [15]. We further remark that the effect of boundary conditions used in the DLVO calculations (i.e., CC versus CP) has a minor effect on the calculated stability ratios. The same observation was made for similar systems previously [23].

### 3.3. Heteroaggregation

Let us now focus on the heteroaggregation between AL and SL particles. Such measurements were hardly ever reported in the literature and they present the main results of the present paper. Stability ratios for heteroaggregation involving the AL and SL particles in the presence of SOS and SDS are shown in Figure 6.

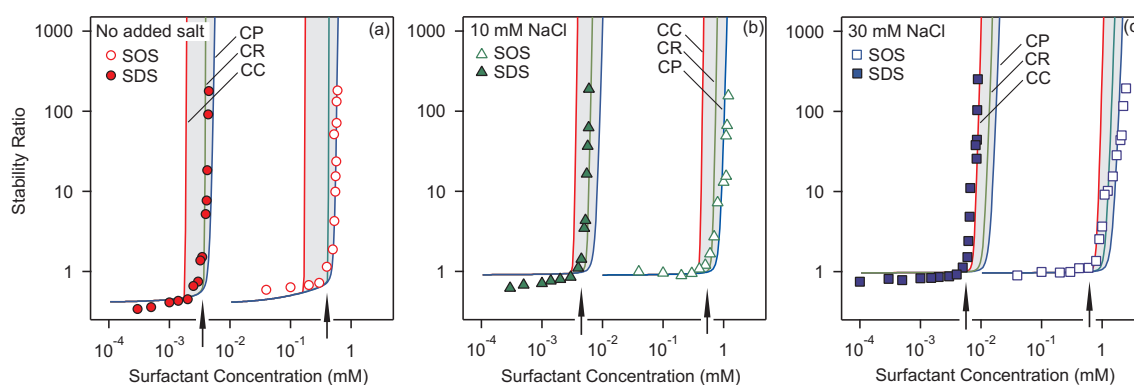


**Figure 6.** Stability ratios for heteroaggregation of AL and SL particles in the presence of SOS and SDS with (a) no added NaCl, (b) 10 mM NaCl, and (c) 30 mM NaCl added. Symbols represent experimental data, while lines show calculations based on DLVO theory. CC, CR, and CP labels mark constant charge, constant regulation, and constant potential boundary conditions. For the CR model the regulation parameters for both particles are equal to 0.5. The IEPs are indicated with arrows.

At low surfactant concentrations, the stability ratio for heteroaggregation is close to unity, and in some cases even below. At these conditions, heteroaggregation is fast. The stability ratios below unity indicate the presence of double-layer attraction between the oppositely charged particles. Their opposite charge is evident from the electrokinetic potentials shown in Figures 3 and 4. However,

the effect of the attractive double-layer forces remains modest and heteroaggregation remains mainly diffusion controlled. As evident from the respective sub-figures, the effect of double-layer attraction is strongest without added salt, and disappears with increasing concentration of the monovalent background electrolyte as observed for oppositely charged particles [6,33]. With increasing surfactant concentration, the stability ratio increases sharply, and the heteroaggregation slows down. This increase in the stability ratio can again be explained by considering the charge of the particles. Above the IEP, the AL particles become negatively charged, and the double layer interaction with the negatively charged SL particles is now repulsive.

The heteroaggregation behavior is similar for both types of surfactants. The stability curves are again shifted to lower concentration for SDS surfactant as compared to SOS. This effect is due to the stronger affinity of SDS to the latex particles than for SOS, which shifts the IEP of the AL particles in the presence of SDS to lower concentrations than for SOS.

The full lines in Figure 6 represent the calculations of stability ratios with DLVO theory. Again CP, CR, and CC boundary conditions are being used. The DLVO theory is able to accurately capture the dependence of stability ratios on the surfactant concentration. One further observes that heteroaggregation is much more sensitive to the boundary conditions than what was the case for homoaggregation [7,34]. In most situations, the surfaces appear to regulate strongly, as indicated by the close match with CP boundary conditions. For the case of SDS, the stability ratios are shifting more towards CC conditions, especially for higher background salt concentrations. For heteroaggregation, the regulation parameter of the particle with smaller magnitude of the charge density strongly affects the stability ratio [7,34]. From the present results, we conclude that the AL particles regulate strongly near the IEP, approximatively close to CP conditions. For SDS at 30 mM of NaCl, however, the AL surface seems to behave closer to CC. One may further note that with increasing NaCl concentration, the stability ratio is less sensitive to effects of charge regulation.

### 3.4. Critical Coagulation Concentration

Let us now analyze the critical coagulation concentrations (CCC) for particles in the presence of ionic surfactants. The CCC is the concentration at which the transition between slow and fast aggregation occurs. Figure 5 suggest the presence of two CCCs for the AL particles. The first CCC (homo-CCC1) is located at low concentrations at the transition from slow to fast aggregation. Upon increasing the surfactant concentration, the aggregation becomes slow again, and this transition marks the position of the second CCC (homo-CCC2). For heteroaggregation, only one transition from fast to slow aggregation occurs (see Figure 6). This position reflects another CCC (hetero-CCC).

These three CCCs are plotted as a function of added salt for SOS and SDS in Figure 7 together with IEPs for the AL particles.

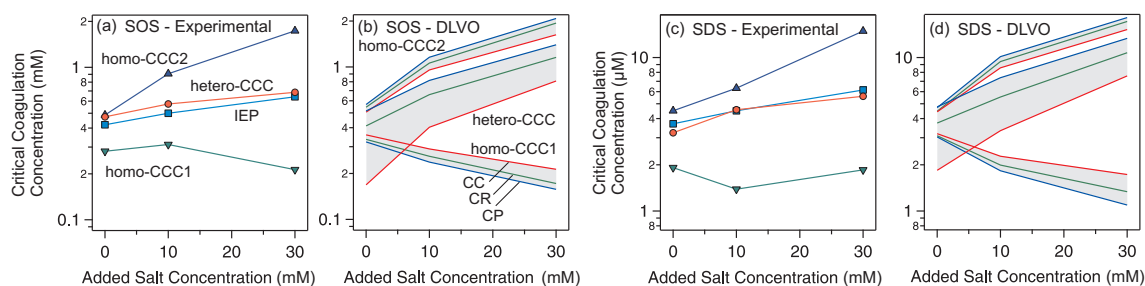


**Figure 7.** Critical coagulation concentration as a function of added salt for (a,b) SOS and (c,d) SDS. Homo-CCC1, homo-CCC2, hetero-CCC, and IEPs of AL particles are presented. The experimental data is shown in (a) and (c), while CCCs extracted from DLVO calculations including the effect of boundary conditions are shown in (b,d). Straight lines are used to connect the respective data points.

One observes that for both surfactants the homo-CCC1 is decreasing slightly with increasing salt concentration, while the homo-CCC2 and hetero-CCC are increasing. The difference between the homo-CCC2 and homo-CCC1 is larger at higher salt concentrations. This observation is in line

with Figure 5, as one observes that the region, where the stability ratio is close to unity, is widening with increasing background salt concentration. This behavior can be understood by inspecting the electrokinetic potentials of AL particles at different added salt concentrations, see Figure 3. The magnitude of these potentials is decreasing with increasing salt concentration. Therefore, the potential needed for re-stabilization is only reached at higher surfactant concentrations, and therefore the homo-CCC2 increases with increasing salt concentration.

The hetero-CCC is always located between the two homo-CCCs and its values are close to the IEP values for AL particles. The position of the hetero-CCC relative to the homo-CCCs can be understood from the the charging curves of the respective particles (see Figures 3 and 4). The AL particles undergo a charge reversal at IEP. They start to aggregate rapidly, when their charge becomes close to neutral, which marks the homo-CCC1. At this point, the heteroaggregation between neutral AL and negatively charged SL particles is still fast. Above the IEP, the AL particles become negatively charged, and the double-layer forces between AL and SL become repulsive, which marks the onset of slow heteroaggregation at hetero-CCC. Finally, when the AL particles become sufficiently highly charged, the homoaggregation of the AL particles also becomes slow, which occurs at homo-CCC2. Therefore, the relative position these three CCCs is mainly determined by the charging of the amidine particles.

The results of the DLVO calculations shown in Figure 7b,d agree very well with the experimentally measured CCCs. In accordance with experiments slight decrease of homo-CCC1 is observed, while homo-CCC2 and hetero-CCC are increasing with increasing salt concentration. One can further observe that the influence of the boundary conditions is the strongest for hetero-CCC, while it is much less pronounced for the two homo-CCCs, especially homo-CCC1. Heteroaggregation is therefore more sensitive on the boundary conditions compared to the homoaggregation [7,34].

While we are unaware of similar measurements of hetero-CCCs, the homo-CCCs were measured earlier for other types of positively charged particles in the presence of alkyl sulfate surfactants. In particular, these studies involve AgI [13,14] and hematite particles [15]. It is instructive to compare the results of these studies with our results.

The first row of Figure 8 shows our measurements for homo-CCCs at different concentration of added salt, while the second row of Figure 8 presents the homo-CCCs with for AgI from Wanatabe [13,14] and Hus et al. [14], and those for hematite by Kobayashi et al. [15]. These CCCs are plotted versus the number of carbons in the alkyl chain. In spite of the different surface chemistry of the different particles, the CCCs systematically decrease with increasing chain length for all three types of particles. This observation is in line with electrophoresis results, where the IEPs are shifted to lower concentrations for surfactants with longer alkyl chains [13,15]. This behavior can be explained by increased tendency for adsorption to solid surfaces for alkyl surfactants increases with increasing chain length. A larger affinity of the surfactants towards the surface induces IEPs at lower concentrations, which induces a similar shift in the CCC. If one further decreases the surfactant chain length, the CCCs further increase, and for very short chain lengths only one CCC is observed [20].

One can further observe that the CCCs for AL and hematite particles are similar, while the ones for AgI particles are higher. Since the position of the CCCs is determined by the affinity of the surfactants for the surface, we suspect that this affinity is comparable for the AL and hematite particles, while it is lower for the AgI particles.

Figure 8a–c shows the effect of added salt on the CCCs. One can observe that by increasing salt concentration the difference between CCC1 and CCC2 is increasing. The area of the region between the CCCs, which marks the fast aggregation regime, is therefore increasing with increasing concentration. The same effect can be seen in the second row of the Figure 8, where thinner fast aggregation areas are observed for AgI particles, which were measured with about 1 mM of added salt, while the fast aggregation regime is wider for hematite particles measured in the presence of 10 mM NaCl.

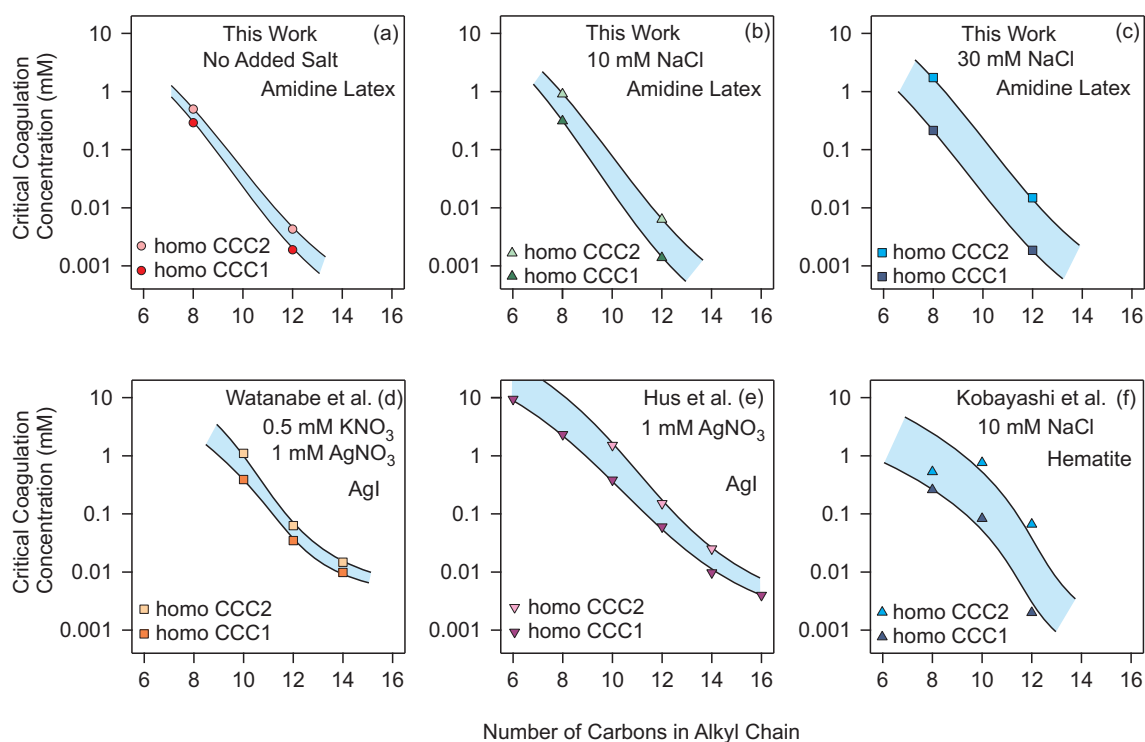


**Figure 8.** Critical coagulation concentration as a function of the chain length of alkyl sulfate surfactant. Homo-CCC1 and homo-CCC2 for amidine latex used in this work with (a) no added salt, (b) 10 mM, and (c) 30 mM salt. AgI particles by (d) Watanabe [13] and (e) Hus et al. [14], and (f) hematite by Kobayashi et al. [15]. The CCCs shown in (e) were extracted from the maxima of turbidity curves given in [14]. The lines serve only as eye-guides. The colored area between the CCCs marks the region of fast aggregation.

#### 4. Conclusions

We investigate the influence of two alkyl sulfate surfactants on homoaggregation and heteroaggregation involving SL and AL particles. Both surfactants SOS and SDS adsorb to both types of particles. The SL particles stay negatively charged and remain stable in the whole range of the surfactant concentration studied. The AL particles are positively charged at low surfactant concentrations, and they undergo a charge reversal with increasing concentration. This charge reversal also dictates the homoaggregation of these particles. The AL particles are stable at low surfactant concentrations, aggregate rapidly close to the charge reversal point, and become re-stabilized at higher surfactant concentrations.

Heteroaggregation between AL and SL particles is fast at low surfactant concentration, where the particles are oppositely charged and the double-layer forces are attractive. Above charge reversal of AL particles, the heteroaggregation becomes slow as the double-layer forces between AL and SL switch from attractive to repulsive.

The affinity of the alkyl sulfate surfactants to the surface increases with increasing length of the alkyl chain. With increasing affinity, the IEP shifts to lower concentrations. The minimum in the stability curves for homoaggregation of the AL particles and the corresponding increase of the stability curve for heteroaggregation are both shifted to lower concentrations, when chain length of the surfactant is increased.

The DLVO theory describes homoaggregation and heteroaggregation processes reasonably well, albeit some discrepancies occur for homoaggregation at low concentrations. The DLVO theory also captures the widening of the fast homoaggregation regime with increasing concentration of NaCl. Charge regulation seems to be close to CP in most cases, except at 30 mM NaCl, where systems behave closer to CC conditions.

**Author Contributions:** Conceptualization, M.B. and G.T.; methodology, T.C., M.B., G.T.; software, M.B. and G.T.; validation, T.C., M.B. and G.T.; formal analysis, T.C., M.B. and G.T.; investigation, T.C., M.B. and G.T.; data curation, T.C., M.B. and G.T.; writing—original draft preparation, G.T.; writing—review and editing, T.C., M.B. and G.T.; visualization, T.C., M.B. and G.T.; supervision, M.B. and G.T.; project administration, M.B.; funding acquisition, M.B. All authors have read and agreed to the published version of the manuscript.

**Funding:** This research was funded by the Swiss National Science Foundation through awards 178759 and 159874 and by the University of Geneva.

**Conflicts of Interest:** The authors declare no conflict of interest.

## References

1. Balzer, B.; Hruschka, M.K.M.; Gauckler, L.J. Coagulation Kinetics and Mechanical Behavior of Wet Alumina Green Bodies Produced via DCC. *J. Colloid Interface Sci.* **1999**, *216*, 379–386. [[CrossRef](#)]
2. Trefalt, G.; Tadić, B.; Kosec, M. Formation of Colloidal Assemblies in Suspensions for Pb(Mg<sub>1/3</sub>Nb<sub>2/3</sub>)O<sub>3</sub> Synthesis: Monte Carlo Simulation Study. *Soft Matter* **2011**, *7*, 5566–5577. [[CrossRef](#)]
3. Farrokhpay, S. A Review of Polymeric Dispersant Stabilisation of Titania Pigment. *Adv. Colloid Interface Sci.* **2009**, *151*, 24–32. [[CrossRef](#)]
4. Volodkin, D.; Ball, V.; Schaaf, P.; Voegel, J.C.; Möhwald, H. Complexation of Phosphocholine Liposomes with Polylysine: Stabilization by Surface Coverage versus Aggregation. *Biochim. Biophys. Acta* **2007**, *1768*, 280–290. [[CrossRef](#)] [[PubMed](#)]
5. Galletto, P.; Lin, W.; Borkovec, M. Measurement of Heteroaggregation Rate Constants by Simultaneous Static and Dynamic Light Scattering. *Phys. Chem. Chem. Phys.* **2005**, *7*, 1464–1471. [[CrossRef](#)] [[PubMed](#)]
6. Lin, W.; Kobayashi, M.; Skarba, M.; Mu, C.; Galletto, P.; Borkovec, M. Heteroaggregation in Binary Mixtures of Oppositely Charged Colloidal Particles. *Langmuir* **2006**, *22*, 1038–1047. [[CrossRef](#)] [[PubMed](#)]
7. Cao, T.; Sugimoto, T.; Szilagyi, I.; Trefalt, G.; Borkovec, M. Heteroaggregation of Oppositely Charged Particles in the Presence of Multivalent Ions. *Phys. Chem. Chem. Phys.* **2017**, *19*, 15160–15171. [[CrossRef](#)]
8. Cao, T.; Trefalt, G.; Borkovec, M. Measuring Slow Heteroaggregation Rates in the Presence of Fast Homoaggregation. *J. Colloid Interface Sci.* **2020**, *566*, 143–152. [[CrossRef](#)]
9. James, R.O.; Homola, A.; Healy, T.W. Heterocoagulation of Amphoteric Latex Colloids. *J. Chem. Soc.-Faraday Trans. I* **1977**, *73*, 1436–1445. [[CrossRef](#)]
10. Kihira, H.; Matijevic, E. Kinetics of Heterocoagulation 3. Analysis of Effects Causing the Discrepancy between the Theory and Experiment. *Langmuir* **1992**, *8*, 2855–2862. [[CrossRef](#)]
11. Imae, T.; Muto, K.; Ikeda, S. The pH Dependence of Dispersion of TiO<sub>2</sub> Particles in Aqueous Surfactant Solutions. *Colloid. Polym. Sci.* **1991**, *269*, 43–48. [[CrossRef](#)]
12. Liang, L.; Morgan, J.J. Chemical Aspects of Iron-Oxide Coagulation in Water: Laboratory Studies and Implications for Natural Systems. *Aquat. Sci.* **1990**, *52*, 32–55. [[CrossRef](#)]
13. Watanabe, A. Physico-Chemical Studies on Surface Active Agents. 2. The Coagulation of Positive Silver Iodide Sols by Anionic Surface Active Agents. *Bull. Inst. Chem. Res. Kyoto Univ.* **1960**, *38*, 179–215.
14. Hus, M.; Kmitel, J.; Herak, M.J. The Influence of Sodium-n-Alkyl Sulphates on Positively and Negatively Charged AgI Systems. *Colloid. Polym. Sci.* **1978**, *256*, 487–489. [[CrossRef](#)]
15. Kobayashi, M.; Yuki, S.; Adachi, Y. Effect of Anionic Surfactants on the Stability Ratio and Electrophoretic Mobility of Colloidal Hematite Particles. *Colloids Surf. A* **2016**, *510*, 190–197. [[CrossRef](#)]
16. Koopal, L.K.; Goloub, T.; de Keizer, A.; Sidorova, M.P. The Effect of Cationic Surfactants on Wetting, Colloid Stability and Flotation of Silica. *Colloids Surf. A* **1999**, *151*, 15–25. [[CrossRef](#)]
17. Hakim, A.; Kobayashi, M. Charging, Aggregation, and Aggregate Strength of Humic Substances in the Presence of Cationic Surfactants: Effects of Humic Substances Hydrophobicity and Surfactant Tail Length. *Colloids Surf., A* **2019**, *577*, 175–184. [[CrossRef](#)]
18. Ottewill, R.H.; Rastogi, M.C. The Stability of Hydrophobic Sols in the Presence of Surface-Active Agents 2. The Stability of Silver Iodide Sols in the Presence of Cationic Surface-Active Agents. *Trans. Faraday Soc.* **1960**, *56*, 866–879. [[CrossRef](#)]
19. Ottewill, R.H.; Rastogi, M.C. The Stability of Hydrophobic Sols in the Presence of Surface-Active Agents 3. An Examination by Microelectrophoresis of the Behaviour of Silver Iodide Sols in the Presence of Cationic Surface-Active Agents. *Trans. Faraday Soc.* **1960**, *56*, 880–892. [[CrossRef](#)]

20. Oncsik, T.; Desert, A.; Trefalt, G.; Borkovec, M.; Szilagyi, I. Charging and Aggregation of Latex Particles in Aqueous Solutions of Ionic Liquids: Towards an Extended Hofmeister Series. *Phys. Chem. Chem. Phys.* **2016**, *18*, 7511–7520. [[CrossRef](#)]
21. Derjaguin, B.; Landau, L.D. Theory of the Stability of Strongly Charged Lyophobic Sols and of the Adhesion of Strongly Charged Particles in Solutions of Electrolytes. *Acta Physicochim: USSR* **1941**, *14*, 633–662. [[CrossRef](#)]
22. Verwey, E.J.W.; Overbeek, J.T.G. *Theory of Stability of Lyophobic Colloids*; Elsevier: Amsterdam, The Netherlands, 1948.
23. Cao, T.; Trefalt, G.; Borkovec, M. Aggregation of Colloidal Particles in the Presence of Hydrophobic Anions: Importance of Attractive Non-DLVO Forces. *Langmuir* **2018**, *34*, 14368–14377. [[CrossRef](#)] [[PubMed](#)]
24. O'Brien, R.W.; White, L.R. Electrophoretic Mobility of a Spherical Colloidal Particle. *J. Chem. Soc.-Faraday Trans. I* **1978**, *74*, 1607–1626. [[CrossRef](#)]
25. Holthoff, H.; Egelhaaf, S.U.; Borkovec, M.; Schurtenberger, P.; Sticher, H. Coagulation Rate Measurements of Colloidal Particles by Simultaneous Static and Dynamic Light Scattering. *Langmuir* **1996**, *12*, 5541–5549. [[CrossRef](#)]
26. Elimelech, M.; Gregory, J.; Jia, X.; Williams, R.A. *Particle Deposition and Aggregation: Measurement, Modeling, and Simulation*; Butterworth-Heinemann Ltd.: Oxford, UK, 1995.
27. Russel, W.B.; Saville, D.A.; Schowalter, W.R. *Colloidal Dispersions*; Cambridge University Press: Cambridge, UK, 1989.
28. Trefalt, G.; Behrens, S.H.; Borkovec, M. Charge Regulation in the Electrical Double Layer: Ion Adsorption and Surface Interactions. *Langmuir* **2016**, *32*, 380–400. [[CrossRef](#)] [[PubMed](#)]
29. Honig, E.P.; Roeberson, G.J.; Wiersema, P.H. Effect of Hydrodynamic Interaction on Coagulation Rate of Hydrophobic Colloids. *J. Colloid Interface Sci.* **1971**, *36*, 97–102. [[CrossRef](#)]
30. Hiemstra, T.; van Riemsdijk, W.H. Effect of Different Crystal Faces on Experimental Interaction Force and Aggregation of Hematite. *Langmuir* **1999**, *15*, 8045–8051. [[CrossRef](#)]
31. Schudel, M.; Behrens, S.H.; Holthoff, H.; Kretzschmar, R.; Borkovec, M. Absolute Aggregation Rate Constants of Hematite Particles in Aqueous Suspensions: A Comparison of Two Different Surface Morphologies. *J. Colloid Interface Sci.* **1997**, *196*, 241–253. [[CrossRef](#)]
32. Lin, W.; Galletto, P.; Borkovec, M. Charging and Aggregation of Latex Particles by Oppositely Charged Dendrimers. *Langmuir* **2004**, *20*, 7465–7473. [[CrossRef](#)]
33. Puertas, A.M.; Maroto, J.A.; Fernandez-Barbero, A.; de las Nieves, F.J. On the Kinetics of Heteroaggregation versus Electrolyte Concentration: Comparison between Simulation and Experiment. *Colloids Surf. A* **1999**, *151*, 473–481. [[CrossRef](#)]
34. Trefalt, G.; Ruiz-Cabello, F.J.M.; Borkovec, M. Interaction Forces, Heteroaggregation, and Deposition Involving Charged Colloidal Particles. *J. Phys. Chem. B* **2014**, *118*, 6346–6355. [[CrossRef](#)] [[PubMed](#)]

**Publisher's Note:** MDPI stays neutral with regard to jurisdictional claims in published maps and institutional affiliations.



© 2020 by the authors. Licensee MDPI, Basel, Switzerland. This article is an open access article distributed under the terms and conditions of the Creative Commons Attribution (CC BY) license (<http://creativecommons.org/licenses/by/4.0/>).